

fmr1 mutation interacts with sensory experience to alter the early development of behavior and sensory coding in zebrafish

Shuyu Zhu,¹ Michael McCullough,¹ Zac Pujic,¹ Jordan Sibberas,¹ Biao Sun,¹
Bianca Bucknall,¹ Lilach Avitan,¹ and Geoffrey J Goodhill^{1,2*}

¹Queensland Brain Institute,

²School of Mathematics and Physics

The University of Queensland, Brisbane, Queensland 4072, Australia

*Corresponding author: g.goodhill@uq.edu.au

1 **Abstract**

2 While Autism Spectrum Disorders (ASDs) are developmental in origin little is known about how
3 they affect the early development of behavior and sensory coding, or how this is modulated by
4 the sensory environment. The most common inherited form of autism is Fragile X syndrome,
5 caused by a mutation in *fmr1*. Here we show that zebrafish *fmr1*^{-/-} mutant larvae raised in a nat-
6 uralistic visual environment display early deficits in hunting behavior, tectal map development,
7 tectal network properties and decoding of spatial stimuli. However when given a choice they
8 preferred an environment with reduced visual stimulation, and rearing them in this environment
9 improved these metrics. Older *fmr1*^{-/-} fish showed differences in social behavior, spending
10 more time observing a conspecific, but responding more slowly to social cues. Together these
11 results help reveal how *fmr1*^{-/-} changes the early development of vertebrate brain function, and
12 how manipulating the environment could potentially help reduce these changes.

13 Introduction

14 Autism spectrum disorders (ASDs) are neurodevelopmental in origin. Increasing evidence sug-
15 gests that a key way in which ASDs alter behavior and cognition is via altering the development
16 of sensory processing [1]. While ASDs can be identified in humans as early as 6 months of age
17 [2], little is known about how the early development of sensory neural processing is altered in
18 ASDs.

19 Fragile X syndrome (FXS) is the most common single-gene cause of autism. It is due
20 to a trinucleotide repeat expansion in the Fragile X mental retardation 1 (*fmr1*) gene, which
21 leads to a lack of its product Fragile X mental retardation protein (FMRP). FMRP is highly
22 expressed in neurons in the brain and regulates many aspects of brain development [3, 4,
23 5, 6]. Characteristics of the human FXS phenotype include low IQ, hyperactivity, attention
24 deficits, and sensory deficits [1, 7, 8]. Changes in sensory processing are common in ASDs
25 [1, 9, 10, 11, 12, 13, 14, 15, 16]. ASD individuals often display impaired adaptation to chronic
26 sensory stimulation [17, 18, 19]. *fmr1*^{-/-} mice have circuit defects in the cortex [20, 21], larger
27 networks of neurons that respond to sensory stimuli [22], and stronger motor responses and
28 impaired adaptation to whisker stimulation [23]. However overall relatively little is known about
29 how the early developmental trajectory of FXS affects behavior and sensory coding, and these
30 are difficult questions to study in very young mammals.

31 In contrast the nervous system of zebrafish develops extremely rapidly, and by 5 dpf
32 (days post-fertilization) larval zebrafish are already able to hunt fast-moving prey using only
33 visual cues [24, 25, 26, 27]. This behavior relies on predictive models of target position [28].
34 Social behaviour begins to develop around 15 dpf and is again largely dependent on visual cues
35 [29]. *nacre* zebrafish (which carry a mutation that affects pigment cells) are transparent at larval
36 stages, and neural activity can be directly visualized non-invasively at large scale yet single-
37 neuron resolution using transgenically encoded fluorescent calcium indicators in an intact and
38 unanaesthetised animal [30, 31]. Zebrafish have a strong genetic and physiological homology
39 to mammals, and their affective, social and cognitive processes are analogous to those seen
40 in rodents and humans [32]. However the effects of *fmr1*^{-/-} mutation on the development of

41 visually-driven behavior and associated neural coding remaining unknown.

42 While the environment has been hypothesized to play an important role in the expres-
43 sion of FXS, conflicting results have been obtained for how sensory experience affects the
44 developmental trajectory of FXS mouse models. While [33] reported that environmental en-
45 richment rescued some abnormalities, in contrast [34] found that enrichment was necessary
46 for differences between the genotypes to be revealed. Since early zebrafish hunting and so-
47 cial behavior are highly visually driven and the complexity of visual stimulation can be easily
48 manipulated, zebrafish provide a new opportunity to address the role of sensory experience in
49 modulating the *fmr1*^{-/-} phenotype.

50 Here we reveal that there is a delay in the early developmental trajectory of *fmr1*^{-/-}
51 compared to *fmr1*^{+/-} zebrafish, reflected by less efficient and successful hunting behaviours
52 at younger ages and delayed maturation of neural coding in the optic tectum. While these met-
53 rics normalised by 14 dpf, a longer-term effect of the mutation was revealed by altered social
54 behavior at 28 dpf. However *fmr1*^{-/-} fish preferred reduced sensory stimulation and, surpris-
55 ingly, raising *fmr1*^{-/-} fish in such an environment moved many of these of these metrics towards
56 the *fmr1*^{+/-} case. Together this work gives new insight into how *fmr1* mutation affects sen-
57 sory development in the vertebrate brain, and provides evidence for an important impact of the
58 environment on the development of FXS.

59 Results

60 ***fmr1*^{-/-} fish display craniofacial alterations**

61 For this study we used the *fmr1*^{-/-} knockout line generated from a TILLING screen by [35]. A
62 characteristic feature of Fragile X syndrome is altered craniofacial structure, including an elon-
63 gated face [36]. While craniofacial alterations were found in zebrafish *fmr1*^{-/-} mutants generated
64 using a morpholino knockdown approach [37], and subsequently in a CRISPR/Cas9 knockout
65 [38], such changes were not originally reported in the knockout of [35]. We revisited this issue
66 by crossing *fmr1*^{+/-} with *fmr1*^{-/-} fish to produce roughly equal numbers of *fmr1*^{-/-} and *fmr1*^{+/-} off-
67 spring, performing Alcian blue staining at 3 developmental ages, and quantitatively comparing
68 facial cartilage structure measurements (Fig. S1a,b). Canonical variate analysis [39] revealed
69 differences in structure with both age (first canonical variable) and genotype (second canonical
70 variable) (Fig. S1c). For the second canonical variable high weights were given for distances
71 quantifying the length of the face (Fig. S1d), and at least two of these distances showed sig-
72 nificant differences between genotypes at 9 and 14 dpf (Fig. S1e,f). In addition the angle of
73 Meckel's cartilage was significantly different between genotypes (Fig. S1g). These results con-
74 firm that craniofacial alterations analogous to human Fragile X syndrome occur in this *fmr1*^{-/-}
75 knockout, providing further support for this line as a relevant model system.

76 **Hunting is less successful in *fmr1*^{-/-} fish**

77 From 5 dpf zebrafish larvae start to hunt small, fast-moving prey such as *Paramecia*. This relies
78 on precise sensorimotor coordination, and hunting success improves over development [27]. To
79 test whether this behavior is altered by *fmr1* mutation, heterozygous and homozygous larvae
80 were placed individually into small dishes with *Paramecia*, and hunting behavior was imaged for
81 10-15 min with a 500 fps camera. We imaged fish at 5, 8-9 and 13-14 dpf (henceforth referred
82 to as 5, 9 and 14 dpf for brevity), and derived average values for hunting metrics across all
83 events for each fish. Fish were genotyped after the experiment. To ensure we only included

84 representative hunting behaviours, we used fish that had more than 7 hunting events across
85 the entire duration of the hunting assay (10th percentile of the distribution of number of events
86 per fish; 9, 10, and 2 fish were rejected by this criterion for ages 5, 9, and 14 dpf respectively,
87 leading to n = 21, 21, 10 for *fmr1*^{-/-} and n = 20, 27, 11 for *fmr1*^{+/-} for ages 5, 9 and 14 dpf
88 respectively; different fish at each age).

89 *fmr1*^{-/-} and *fmr1*^{+/-} fish had similar gross motor function: fish length, speed, proportion
90 of time stationary, number of bouts to strike, duration to strike and inter-bout interval were all
91 indistinguishable between *fmr1*^{-/-} fish and *fmr1*^{+/-} fish (Fig. S2; these measures did though
92 change with age, consistent with [27]). However *fmr1*^{-/-} fish at 5 and 9 dpf were less successful
93 at hunting than *fmr1*^{+/-} fish, as evidenced by a lower hit rate (the fraction of successful prey
94 captures out of all hunting events recorded per fish) (Fig. 1a), and higher abort rate (the fraction
95 of abort events out of all hunting events recorded per fish, where an abort event means that the
96 fish pursued the Paramecium of interest but aborted the pursuit and never struck at the prey)
97 (Fig. 1b). 5- and 9-dpf *fmr1*^{-/-} fish also showed a preference for hunting paramecia at more
98 peripheral angles in the visual field (Fig. 1c) than *fmr1*^{+/-} fish, as measured by the position of
99 the target paramecium when eye convergence occurred, indicating the start of the hunting event
100 (Fig. 1d). Together, these results demonstrate an initial delay in the development of effective
101 hunting behavior *fmr1*^{-/-} fish, and suggest an altered hunting strategy in these fish.

102 **Stimulus-driven responses are slower to develop in *fmr1*^{-/-} fish**

103 In light of the changes in hunting in *fmr1*^{-/-} fish observed above, we asked if *fmr1* mutation
104 altered early development of spontaneous and evoked activity in the optic tectum, a brain region
105 critical for successful hunting [40]. Fish aged at 5, 9 and 14 dpf (*fmr1*^{-/-}, n = 10, 12, 6; *fmr1*^{+/-},
106 n = 11, 12, 6 respectively) were embedded in low melting point agarose, and 2-photon imaging
107 was used to record calcium signals from the tectum in a plane 70 μm below the skin [27]. Each
108 fish was imaged first in the dark for 30 min of spontaneous activity (SA), followed by a 5 min
109 adjustment period, and then in response to prey-like, 6° stationary spots at 9 positions in the
110 visual field ranging from 45° to 165° in 15° increments. Each stimulus was presented for 1 s

111 followed by a 19 s gap, with 20 repetitions of each stimulus in pseudo-random order. For some
112 later analyses divided the data recorded for the stimulated period into activity from stimulus
113 onset to 5 s post onset, ('evoked activity', EA) and activity from 15 s post-stimulus onset to the
114 time of the next stimulus ('spontaneous within evoked', SE).

115 The tectum is topographically organised with the anterior portion responding to the frontal
116 visual field, and the posterior portion responding to the rear visual field (Fig. 2a). However previ-
117 ous work with wild type fish has shown that the tectal representation of visual space at this tectal
118 depth develops non-uniformly: responses are initially weaker and neural decoding worse in the
119 anterior tectum, but by 13-15 dpf the representation has become uniform across the visual field
120 [27]. We therefore asked if this developmental trajectory is altered in *fmr1*^{-/-} fish. Responses
121 in *fmr1*^{-/-} fish were also topographically organised (Fig. 2b). However tectal development, as
122 measured by the spatial uniformity of preferred stimuli, was initially delayed in *fmr1*^{-/-} fish (Fig.
123 2c). The area under these curves was significantly smaller for *fmr1*^{-/-} fish compared to *fmr1*^{+/-}
124 fish at 5 dpf, but equalised at later ages (Fig. 2d). The proportion of stimulus selective cells
125 (those responsive to any stimulus) was lower for *fmr1*^{-/-} compared to *fmr1*^{+/-} fish at 9 dpf (Fig.
126 2e). Also, the proportion of tectal neurons responding to different visual angles was initially
127 biased towards the rear visual field but became more evenly distributed over development for
128 both *fmr1*^{-/-} and *fmr1*^{+/-} fish, similar to wild-type fish [27]. However at 5 dpf this bias was sig-
129 nificantly more pronounced for *fmr1*^{-/-} than *fmr1*^{+/-} fish (Fig. 2f, 2g), again suggesting an initial
130 developmental delay.

131 Thus at the level of individual neurons, *fmr1*^{-/-} fish displayed an altered developmental
132 trajectory of tectal spatial representation.

133 **Neural assemblies and neural coding are altered in *fmr1*^{-/-} fish**

134 Neural assemblies have been proposed to serve critical roles in neural computation [41]. We
135 next identified tectal neural assemblies using the graph clustering algorithm introduced in [42]
136 (Fig. 3a) and tested for alterations in assembly structure. For stimulus-evoked assemblies (EA)

137 the number of neurons per assembly was greater for *fmr1*^{-/-} than *fmr1*^{+/-} fish at 9 dpf (Fig. 3b),
138 suggesting higher excitability in *fmr1*^{-/-} fish. However at 5 dpf assemblies in *fmr1*^{-/-} fish were
139 more compact, i.e. had a reduced span of their projection onto the AP axis of the tectum (Fig.
140 3c).

141 These results suggest a delayed development of neural coding in the tectum. One mea-
142 sure of the quality of neural coding is decoding performance; in this case, how accurately stim-
143 ulus position can be decoded from tectal activity. Decoding was worse for several visual field
144 positions at 5 dpf for *fmr1*^{-/-} fish, but this equalised over development (Fig. 3d-3e). Thus overall
145 the developmental trajectory of tectal coding was altered in *fmr1*^{-/-} fish, and displayed an initial
146 delay relative to *fmr1*^{+/-} fish.

147 **Correlation structures and synchronised activity patterns are altered in** 148 ***fmr1*^{-/-} fish**

149 How are tectal network properties altered by *fmr1* mutation? During EA epochs short range
150 correlations were higher for *fmr1*^{-/-} fish (Fig. 4a), though similar for SA epochs (Fig. 4b).
151 By thresholding the SA and EA correlation matrices and determining their degree of similarity
152 (Hamming distance), we found that these matrices were less similar for 5 dpf *fmr1*^{-/-} fish (Fig.
153 4c). At 9 dpf there was an increase in coactivity level (mean number of neurons active together)
154 in *fmr1*^{-/-} fish for EA epochs (Fig. 4d). At 9 dpf EA epochs for *fmr1*^{-/-} fish had higher dimen-
155 sionality, as measured by the Participation Ratio [43] (Fig. 4e). The residuals for both SA and
156 SE patterns when projected onto the EA space (see Methods) were larger in *fmr1*^{-/-} fish at 9
157 dpf (Fig. 4f), suggesting EA patterns in these fish were geometrically less similar to SA patterns
158 than in *fmr1*^{+/-} fish. However, we did not observe such differences at 5 or 14 dpf (Fig. S3).

159 Thus at early ages compared to *fmr1*^{+/-} fish, *fmr1*^{-/-} fish had higher correlations be-
160 tween neurons, decreased similarity between evoked and spontaneous activity patterns, higher
161 coactivity levels and higher-dimensional activity, consistent with increased excitability. However
162 these properties had mostly equalised by 14 dpf, suggesting a transient period of disorder in

163 network properties during development.

164 **Reduced sensory stimulation during development improves outcomes for** 165 ***fmr1*^{-/-} fish**

166 For the experiments described thus far the fish were raised in petri dishes placed on a gravel
167 substrate [44] (see Methods), which is a more natural visual environment than featureless petri
168 dishes, and is indeed preferred by adult wild-type fish [45]. However humans with ASDs often
169 experience sensory over-responsivity to normal sensory environments, sometimes accompa-
170 nied by aversive behaviours [46]. We therefore wondered whether *fmr1*^{-/-} larvae would prefer
171 an environment with reduced sensory stimulation, and whether rearing in such an environment
172 would change developmental outcomes for these fish.

173 First we compared free-swimming behavior (no prey items) for *fmr1*^{-/-} and WT fish at
174 8-9 dpf in 85 mm dishes, where half of each dish had an image of a gravel substrate on the
175 bottom and the other half was featureless (uniform brightness equal to the mean brightness of
176 the gravel half of the dish) (Fig. S4a). WT fish displayed no preference for either side of the
177 dish. However *fmr1*^{-/-} fish spent significantly more time on the featureless side of the dish (Fig.
178 5a), consistent with the hypothesis of an active avoidance of sensory stimulation. This was true
179 both for fish raised to that point on gravel, and fish raised in a featureless environment (Fig.
180 S4b).

181 Next, we compared our original cohort of *fmr1*^{-/-} fish raised on gravel (now termed *fmr1*^{-/-}
182 /-(N), for ‘naturalistic stimulation’) with a new cohort of *fmr1*^{-/-} fish raised in featureless dishes
183 (termed *fmr1*^{-/-}-(R), for ‘reduced stimulation’), in order to determine whether the sensory en-
184 vironment could affect the expression of the *fmr1*^{-/-} phenotype (n = 9, 14, 6 for 5, 9, 14 dpf
185 respectively). Statistical comparisons are presented between *fmr1*^{-/-}-(N) and *fmr1*^{-/-}-(R) fish, but
186 the data discussed earlier for *fmr1*^{+/-}-(N) fish is also shown again for comparison.

187 When assessed using the same featureless chambers as before, hunting success (hit

188 ratio) was significantly improved at 9 dpf for *fmr1*^{-/-}(R) compared to *fmr1*^{-/-}(N) fish (Fig. 5b).
189 This was primarily driven by a decrease in the abort ratio for *fmr1*^{-/-}(R) fish (Fig. 5c). However
190 at 5 dpf the abort rate for *fmr1*^{-/-}(R) fish was higher than *fmr1*^{-/-}(N) fish, despite there being
191 no difference in hit rate, suggesting that *fmr1*^{-/-}(R) fish had difficulty sustaining hunting events
192 at this early age. We found that across a range of ages *fmr1*^{-/-}(R) fish were more efficient at
193 hunting, as measured by inter-bout interval during a hunting sequence (Fig. 5d), number of
194 bouts prior to a strike (Fig. 5e), and duration to strike (Fig. 5f).

195 Reduced sensory stimulation also altered tectal responses in *fmr1*^{-/-} fish. At 9 dpf neu-
196 rons in *fmr1*^{-/-}(R) fish were less excitable (Fig. 6a) with smaller tuning widths (Fig. 6b). 9
197 dpf *fmr1*^{-/-}(R) fish also had fewer neurons per EA and SA assembly than *fmr1*^{-/-}(N) fish (Fig.
198 6c,6d). *fmr1*^{-/-}(R) fish had less compact EA assemblies at 5-dpf *fmr1*^{-/-}(R) fish compared to
199 *fmr1*^{-/-}(N) fish (Fig. 6e). At 9 dpf coactivity levels in *fmr1*^{-/-}(R) fish were lower than *fmr1*^{-/-}(N)
200 fish during EA epochs (Fig. 6f). We also found that both SA and SE patterns in *fmr1*^{-/-}(R) fish
201 were geometrically more similar at 9 dpf to EA patterns compared to *fmr1*^{-/-}(N) fish (Fig. 6g).
202 For all these metrics the *fmr1*^{-/-}(R) fish were closer to the *fmr1*^{+/-}(N) fish than were *fmr1*^{-/-}(N)
203 fish. Thus reduced sensory stimulation during development reduced the impact of the *fmr1*
204 mutation.

205 **Social behaviour is altered in *fmr1*^{-/-} fish**

206 For many of the metrics examined above, by 14 dpf *fmr1*^{-/-} fish are indistinguishable from
207 *fmr1*^{+/-} fish. Does this mean that the effects of *fmr1* mutation in zebrafish are only transient?
208 A key behavior that emerges at later ages is social interaction. We therefore asked whether
209 there are any differences in social behavior between *fmr1*^{-/-} and WT fish, at both 13-14 dpf
210 and 26-28 dpf (WT: n = 36, 88, *fmr1*^{-/-}: n = 48, 80 respectively; for simplicity we will refer to
211 these as just 14 and 28 dpf respectively; these fish were raised in 1 L tanks in the University
212 of Queensland's central aquarium). For these experiments we used a U-shaped behavioral
213 chamber similar to that of [47] (Fig. 7a,b), and compared how the movements of *fmr1*^{-/-} versus
214 WT test fish were affected by the presence of a WT cue fish in one arm of the chamber over an

215 imaging time of 30 min. To avoid potential effects on social behaviour caused by differences in
216 physical appearance, both WT and *fmr1*^{-/-} fish were in nacre background and the cue fish was
217 size matched to the test fish.

218 At both 14 and 28 dpf, *fmr1*^{-/-} fish travelled a greater distance in the chamber than
219 WT fish (Fig. 7c). This is consistent with hyperactivity of *fmr1*^{-/-} fish as reported previously
220 [48, 49]. As an initial measure of social interaction we calculated the social preference index
221 (SPI) as in [47], which measures the proportion of time the fish spends in the arm of the chamber
222 containing the cue fish versus the empty arm. Neither genotype displayed a preference between
223 arms at 14 dpf (Fig. 7d), but by 28 dpf both genotypes showed a preference for the arm
224 containing the cue fish. Surprisingly however, at 28 dpf *fmr1*^{-/-} fish had a stronger preference
225 than WT fish for the arm containing the cue fish, suggesting a greater desire for social interaction
226 (Fig. 7d).

227 When cue and test 28-dpf fish could see each other they tended to respond to each
228 other's movements, with sometimes the test fish leading and sometimes the cue fish leading
229 (Fig. 7e). This behavior was not present at 14 dpf (Fig. 7f, 7g). However by 28 dpf *fmr1*^{-/-} fish,
230 unlike WT fish, showed a clear asymmetry between their behavior and that of the cue fish. In
231 particular, *fmr1*^{-/-} fish took on average 26 ms longer than WT fish to respond to movements of
232 the test fish (Fig. 7h). Thus it appears that, although *fmr1*^{-/-} fish have greater desire for social
233 interaction than WT fish, they interact less effectively.

234 Discussion

235 Previous studies of zebrafish mutant for *fmr1* have shown a variety of phenotypic effects. Using
236 a morpholino approach [37] reported changes in craniofacial structure and increased axonal
237 branching during development. The initial description of the knockout line used in the present
238 work did not find similar changes [35], which has led to doubts about the relevance of this line
239 for studying FXS [38]. However [35] did not report quantitative results for craniofacial structure.
240 Our more detailed and rigorous analysis demonstrates that craniofacial abnormalities do indeed

241 exist in this line (Fig. S1). Using this line [50] showed changes in open-field behavior in adult
242 *fmr1*^{-/-} fish, [51] showed increased axonal branching early in development, and [52] showed
243 abnormal auditory processing. Using adults from a different *fmr1* knockout line, [48] showed
244 changes in exploratory behavior, avoidance learning, long-term potentiation and long-term de-
245 pression. Using a *fmr1* knockout generated via CRISPR/Cas9, [38] showed that 5 dpf fish
246 had craniofacial changes, hyperactivity, and changes in response to light stimulation. Here we
247 have significantly extended these previous analyses of the *fmr1* knockout by examining hunting
248 and social behavior, tectal coding, how these change across development, and how the visual
249 environment can alter the expression of the *fmr1* knockout phenotype.

250 In terms of tectal activity we found an altered developmental trajectory of tectal spatial
251 representation and tectal coding in *fmr1*^{-/-} fish, including higher correlations and coactivity lev-
252 els at younger ages. Many of these changes mirror those seen previously in *fmr1*^{-/-} mouse
253 cortex [20, 53], supporting the relevance of zebrafish model. These include larger short-range
254 neuron-neuron correlations at young ages, and larger numbers of neurons recruited to peaks
255 of synchrony (analogous to our neural assemblies). A leading hypothesis for the underlying
256 cause of some of these changes is an increase in neural excitation (E) relative to inhibition (I),
257 i.e. E-I balance [54]. Supporting this, inhibitory interneurons have been implicated in network
258 dysfunction in FXS [55, 56, 57, 58]. A recent suggestion is that E-I balance changes are in fact
259 compensatory in ASDs, helping to restore the system to a normal operating point [59]. Inhibitory
260 neurons in zebrafish tectum have been identified using a variety of molecular techniques. For
261 instance, [60] found that almost all *d/xc5*-positive neurons in the tectum are GABAergic, and that
262 this population comprises 5 - 10% of all tectal neurons. While alterations in E-I balance in *fmr1*^{-/-}
263 zebrafish remain to be investigated, an intriguing hypothesis raised by our work is that any
264 such changes are modulated by the environment in which the animals are raised.

265 Our behavioral data shows that, at younger ages, *fmr1*^{-/-} fish are worse hunters than
266 *fmr1*^{+/-} fish under naturalistic rearing conditions. Given the changes we observed in tectal
267 activity, this is consistent with findings from mice [61, 62] and humans [2, 9, 11, 12, 14, 63]
268 that *fmr1* mutation introduces low-level visual deficits. However, according to some metrics,
269 *fmr1*^{-/-} fish raised with reduced sensory stimulation were better at prey capture than *fmr1*^{-/-}

270 raised under naturalistic conditions. It should be noted though that all prey-capture assays
271 were performed in relatively featureless dishes, a similar visual environment to the reduced
272 sensory stimulation rearing case. This could potentially place fish raised under naturalistic
273 conditions at a disadvantage in our prey capture assay, since they have adapted to hunting
274 in a richer visual environment than the reduced stimulation case. This would be potentially
275 analogous to recent reports that whether zebrafish first experience dry or live food influences
276 their subsequent behavior and brain development [64, 65].

277 For efficiency our primary comparisons were between *fmr1*^{-/-} and *fmr1*^{+/-} fish, both gen-
278 erated from crossing *fmr1*^{-/-} and *fmr1*^{+/-} fish. For our neural imaging experiments we could
279 only examine one fish per day, and the genotype could only be determined after each imag-
280 ing or behavioral experiment using PCR. Thus crossing *fmr1*^{-/-} with *fmr1*^{+/+} fish to additionally
281 compare *fmr1*^{-/-} and *fmr1*^{+/-} with *fmr1*^{+/+} would have required twice as many experiments to
282 obtain the same n values per group. Whether a comparison of *fmr1*^{-/-} and *fmr1*^{+/+} fish would
283 yield stronger or additional phenotypic differences according to the measures we have exam-
284 ined remains a question for future work; however this caveat does not weaken our conclusions
285 regarding differences we have observed between *fmr1*^{-/-} and *fmr1*^{+/-} fish.

286 A common symptom of human FXS is sensory hypersensitivity, which can lead to sen-
287 sory defensiveness [66]. Consistent with visual hypersensitivity we found that *fmr1*^{-/-} fish, unlike
288 *fmr1*^{+/-} fish, preferred to swim in an environment with reduced visual stimulation compared to
289 naturalistic conditions. This is analogous to findings of tactile defensiveness in *fmr1*^{-/-} mice
290 [23]. Furthermore, tectal neurons in our *fmr1*^{-/-} fish showed trends towards higher response
291 probability, and a larger number of neurons per assembly for evoked activity. However, reduc-
292 ing visual stimulation during development moved several metrics of behavior and tectal coding
293 closer to those of *fmr1*^{+/-} raised in a naturalistic environment. A comparison can be made with
294 studies of *fmr1*^{-/-} mice examining the effects of environmental enrichment (EE) (e.g. running
295 wheels and toys). [33] showed that EE largely rescued symptoms of hyperactivity, open-field
296 exploration, habituation and changes in dendritic structure compared to mice reared in the nor-
297 mal lab environment [33], and a subsequent study showed restoration of long-term potentiation
298 in prefrontal cortex to wild type levels [67]. While this would appear to conflict with our results for

299 zebrafish, more recent work found that hippocampal spine morphology was more different be-
300 tween *fmr1* and WT mice after EE [34]. These authors suggested that EE allows for the impact
301 of loss of *fmr1* to be more fully expressed, which is more consistent with our findings. Overall
302 our work suggests an important role for the sensory environment in modulating the effects of
303 loss of *fmr1*^{-/-}, with potential implications for therapies.

304 Many of the differences in prey capture and neural properties we observed in *fmr1*^{-/-}
305 fish occurred at 9 dpf. A previous study of the development of spontaneous neural activity in
306 zebrafish tectum suggested that major reorganisations of tectal networks may be occurring just
307 before this, at 5-6 dpf [42]. Assuming that lack of *fmr1* takes some time to manifest, this would be
308 consistent with observing changes slightly later. Interestingly many of these properties became
309 indistinguishable between genotypes at 14 dpf. However this does not mean that the system
310 had necessarily returned to a normal developmental trajectory by this age. First, we observed
311 changes in social behavior at 28 dpf, even though these were not apparent at 14 dpf. Second, it
312 has been argued that a misregulation of critical periods can have very long-lasting effects [68].
313 The loss of a particular gene product can result in compensatory regulation of other genes, but
314 this compensation takes time, meaning that critical windows for time-sensitive developmental
315 events may be missed. This hypothesis explains why overall the system may ultimately not
316 function normally, even though some aspects which are initially delayed eventually catch up.

317 We found that by 28 dpf *fmr1*^{-/-} fish display a greater preference for social interaction
318 with a cue fish than *fmr*^{+/-} fish. This is initially surprising, given the well-documented tendency
319 in ASDs in general for reduced social interaction [69]. However, recent work suggests that FXS
320 may diverge from typical ASDs in this regard. In particular, [70] found in an eye-gaze paradigm
321 that individuals with FXS did not show the large reductions in social interest characteristic of
322 idiopathic ASDs. On the other hand, we also found a reduced effectiveness of social interaction
323 in *fmr1*^{-/-} fish, in terms of a slower response to movements of the cue fish. This could potentially
324 be simply a motor deficit, but we found no direct evidence for motor deficits in *fmr1*^{-/-} fish in the
325 prey-capture assay. The altered interaction efficiency observed here is consistent with a recent
326 report of deficits in imitating conspecific behaviour in *fmr1*^{-/-} mice [71]. A more likely explanation
327 is an alteration in information processing in the networks underlying social interaction [72, 73],

328 and analysing these in *fmr1*^{-/-} fish is an interesting direction for future work.

329 Together our results reveal many previously unknown differences in natural behavior in
330 *fmr1*^{-/-} fish, and neural bases for these behavioral changes in terms of altered neural coding.
331 The changes in the developmental trajectory of *fmr1*^{-/-} fish depending on the complexity of the
332 sensory environment, with a less complex environment leading to better outcomes, offers a
333 new direction for future work, potentially leading to novel concepts for therapeutic intervention.
334 Overall, our work suggests new avenues for revealing the developmental alterations of neural
335 systems in neurodevelopmental disorders.

336 **Materials and Methods**

337 **Zebrafish**

338 All procedures were performed with the approval of The University of Queensland Animal
339 Ethics Committee. Fish with the *fmr1*^{hu2787} mutation were originally generated by the Ketting
340 laboratory [35], and obtained for this study from the Sirotkin laboratory (State University of New
341 York). We first in-crossed the mutant line to generate nacre *fmr1*^{hu2787} mutants. For calcium
342 imaging and hunting assay experiments these nacre *fmr1*^{hu2787} mutants were crossed with nacre
343 zebrafish expressing the transgene *HuC:H2B-GCaMP6s* to give pan-neuronal expression of
344 nuclear-localised GCaMP6s calcium indicator. *fmr1*^{+/-} were then crossed with *fmr1*^{-/-} fish (with
345 no consistent relationship between the genotype and the sex of the parent) to produce roughly
346 equal numbers of *fmr1*^{+/-} and *fmr1*^{-/-} offspring. For social behaviour assays nacre *fmr1*^{hu2787}
347 mutants were used.

348 Fish embryos were raised in E3 medium (5mM NaCl, 0.17mM KCl, 0.33mM CaCl₂,
349 0.33mM MgCl₂) at 28.5° C on a 14/10 h light/dark cycle. For the data in Figs 1-6 Fish were kept
350 in small groups in 100 mm petri dishes. For fish raised in a naturalistic sensory environment,
351 petri dishes were placed on top of gravel of average size 15 mm [44]. For fish raised in reduced
352 sensory stimulation environment, the petri dishes were placed on plain stainless wire shelves.

353 All fish were placed into their designated sensory environment within 24 h after fertilisation. As
354 a robust way of handling clutch-to-clutch variability for the results shown in Figs 1-6 only one
355 fish from each clutch at each age was assayed. Thus, clutch-to-clutch variability contributed
356 random noise to the data, but no systematic effect.

357 For the social assay experiments (Fig 7), fish embryos (either WT or *fmr1*^{-/-}) were raised
358 in The University of Queensland aquatic facility until the day before the experiment. Larvae
359 were obtained from 1 L tanks where several males and females were placed together, fed with
360 live rotifers, and used at random without attempting to identify which clutch they came from. The
361 day before imaging about 30 larvae were transported to the lab and kept in a 28.5 °incubator
362 until the imaging session. All test fish were paired with size- and age-matched WT fish. This
363 process was repeated 5 times for each condition and the data combined.

364 **Alcian blue staining**

365 Zebrafish larvae were anaesthetised with ethy-3-aminobenzoate (Sigma Aldrich), fixed
366 overnight in 4% PFA/PBS and then washed three times for 10 minutes in PBS. After bleaching
367 in 3% H₂O₂/0.5% KOH for 1 hour, larvae were rinsed in 70% ethanol and then stained for 45
368 minutes using fresh, filtered, alcian blue stain (0.1% alcian blue, 1% HCl, 70% ethanol and
369 120 mM MgCl₂). Larvae were washed through 70, 50 and 25% ethanol (all containing 10 mM
370 MgCl₂) followed by overnight rinse in 25 and 50% glycerol (all with 0.1% KOH). Larvae were
371 mounted in 100% glycerol and photographed with a Zeiss StereoDiscovery V8 microscope and
372 HRc camera using Zen software.

373 We selected 6 landmarks on the ventral view of the fish and 3 landmarks on the lateral
374 view. In the ventral view, point 1 was defined by the anterior point of Meckel's cartilage, points
375 2 and 3 as the posterior most points of the left and right component of Meckel's cartilage, point
376 4 as the junction of the left and right components of the ceratohyal cartilage, and points 5 and
377 6 as the posterior most points of the left and right components of the ceratohyal cartilage. To
378 compare the overall morphological differences between the two genotype, we calculated the
379 pairwise distances between the ventral view landmarks and applied canonical variate analysis
380 (CVA) using MATLAB's built-in function *canoncorr*. For this computation the genotype variable

381 was represented as binary number, either 0 or 1. The age was rescaled to the range [0,1] so
382 that the canonical coefficients for age and genotype had matching scales and could therefore
383 be directly compared. In lateral views, point 7 was the anterior end of Meckel's cartilage, point 8
384 the junction of Meckel's cartilage and the palatoquadrate, and points 8 and 9 define the lateral
385 axis of the palatoquadrate. Meckel's cartilage angle (MCA) was measured as the angle between
386 7-8 and 8-9.

387 **Hunting behaviour assay**

388 Individual fish were placed into a feeding chamber (CoverWell Imaging Chambers, cat-
389 alogue number 635031, Grace Biolabs) filled with E3 medium and 30-35 paramecia (*Parame-*
390 *cium caudatum*). The chamber was placed onto a custom made imaging stage consisting of a
391 clear-bottom heating plate at 29.5° C, an infrared LED ring (850 nm, 365 LDR2-100IR2-850-LA
392 powered by PD3-3024-3-PI, Creating Customer Satisfaction (CCS) Inc., Kyoto, Japan) below,
393 and a white LED ring (LDR2-100SW2-LA, CCS) above. Images were recorded using a CMOS
394 camera (Mikrotron 4CXP, Mikrotron) at 500 fps using StreamPix (NorPix, Quebec). Recording
395 of hunting behaviour started after the first attempt for feeding was made by the fish, and each
396 fish was then recorded for 10-15 mins.

397 **Analysis of feeding events**

398 The times at which hunting events began in the recordings were identified manually
399 based on eye convergence [24]. Events were then manually classified based on whether the fish
400 aborted pursuit of the target paramecium (abort event, score 0), pursued but failed to capture
401 the target (miss event, score 1), or the fish successfully captured the target (hit event, score 2
402 for capture but then eject, 3 for fully capture). Event end was determined by eye deconvergence
403 for abort events, and for other events by the end of the strike bout. The target paramecium was
404 defined as the nearest paramecium towards which the first tuning bout was made.

405 Automated tracking of the fish and paramecia was performed using custom image pro-
406 cessing software in MATLAB as detailed in [27] with minor modifications. In brief, frames were
407 first pre-processed to remove the static background using a Gaussian background model. The

408 approximate location of the fish was identified by connected components analysis on the result-
409 ing foreground mask. The position and orientation of the fish were calculated by tracking the
410 midpoint between the eyes and the centre of the swim bladder. This was achieved using a set of
411 correlation filters [74] on pixel values and histogram of oriented gradients features [75]. Filters
412 were rotated through 0,5,10,...,360 degrees and scaled through 60,65,70,...,100% with respect
413 to maximum fish length to accomodate for changes in heading angle and pitch respectively.
414 Filters were trained by manual annotation of the two tracking points in ten randomly selected
415 frames for each fish.

416 Detection of paramecia was performed using connected components analysis to extract
417 the location of prey-like blobs in each frame from the foreground mask. Multi-object tracking of
418 paramecia between frames was achieved using Kalman filtering and track assignment, which
419 enabled tracking through collisions and short periods of occlusion.

420 Bout timings and tail kinematics were calculated by first performing morphological thin-
421 ning and third-order Savitsky-Golay smoothing to extract 101 evenly spaced points along the
422 midline of the tail. Individual bouts were segmented by applying a manually-selected threshold
423 to the amplitude envelope of the mean angular velocity of the most caudal 20% of tail points.
424 Prior to applying the threshold, the angular velocity time series was smoothed using a low-pass
425 filter. The amplitude envelope was estimated using a Hilbert transformation.

426 From the manual annotations and tracking results, we extracted measures to charac-
427 terise the hunting efficiency. Abort ratio was calculated as the percentage of aborted events.
428 Hit ratio was calculated as the percentage of events for which the fish successfully captured the
429 prey in its mouth. Inter-bout time was calculated as the average time between the initiation of
430 feeding related bouts. Detection angle was determined as the angle between the vector defined
431 by the eye midpoint to the target paramecium and the heading angle of the fish.

432 **2-photon calcium imaging**

433 Larvae were embedded in 2.5% low-melting point agarose in the centre of a 35 mm di-
434 ameter petri dish. Calcium signals in the contralateral tectum to the visual stimulation were

435 recorded with the fish upright using a Zeiss LSM 710 2-photon microscope at the Queens-
436 lande Brain Institute's Advanced Microscopy Facility. Excitation was via a Mai Tai DeepSee
437 Ti:Sapphire laser 463 (Spectra-Physics) at an excitation wavelength of 930-940 nm. Emitted
438 signals were bandpassed (500-550 nm) and detected with a nondescanned detector. Images
439 (416 x 300 pixels) were acquired at 2.2 Hz.

440 Fish were first imaged for 30 mins in the dark for spontaneous activity (SA). We then
441 recorded tectal responses to stationary 6° diameter dark spots at an elevation of approximately
442 30° to the fish at either 9 or 11 different horizontal locations (45° to 165° in 15° steps in the
443 first case and 15° to 165° 45 in 15° steps in the second case, where the heading direction of
444 the fish is define as 0°). Only responses to the 9 locations common to all fish were analysed
445 here. Each spot was presented for 1 s followed by 19 s of blank screen a total of 20 times. The
446 presentation order of spot location was randomised, but ensuring that spatially adjacent stimuli
447 were never presented sequentially.

448 **Analysis of neural responses**

449 *Pre-processing of calcium imaging data:* Cell detection and calcium trace extraction were
450 performed using custom MATLAB software as described in [42]. In brief, x-y drifts were cor-
451 rected using a rigid imaging registration algorithm. Active pixels were identified as pixels that
452 showed changes in brightness over the recording to create an activity map. This activity map
453 was then segmented using a watershed algorithm. For each segmented region, the correla-
454 tion coeffiecient between pairs of pixels were calculated. Then, a gaussian mixture model was
455 applied to identify the threshold correlation level for assigning highly correlated pixels to a cell,
456 requiring each cell to contain at least 26 pixels. Once the cells had been identified, we cal-
457 culated the average brightness of the pixels as the raw fluorensence level $F(t)$. The baseline
458 fluorescence was calculated as a smoothed curve fitted to the lower 20% of the values and
459 the instantaneous baseline level $F_0(t)$ was taken as the minimum value of the smoothed traced
460 within 3 s centered at t. Neuronal activity levels were calculated as the change of fluorensence
461 level from the baseline as $\Delta F/F(t) = (F(t)-F_0(t))/F_0(t)$. We defined the mean $\Delta F/F(t)$ over 4 - 7
462 frames post stimulus presentation as the stimulus-evoked response.

463 *Tuning curve:* For each neuron, the average responses to each stimulus were averaged
464 to represent the mean response to the given stimulus. We then applied cubic spline interpola-
465 tion to estimate response amplitude in 5° steps between presented stimuli angles. A Gaussian
466 function was fitted to this interpolated curve to estimate the tuning curve. Neurons with fitted
467 adjusted R^2 larger than 0.7 and a maximum evoked response amplitude larger than $1\Delta F/F(t)$
468 were deemed selective neurons and included in further analysis. From the fitted tuning curve,
469 we also obtained the preferred tuning angle and tuning width for each tuned neuron.

470 *Assembly properties:* Assemblies were detected as detailed previously [42, 76]. In brief,
471 we used a graph theory-based approach to automatically detect assemblies without prior as-
472 sumptions of expected number of assemblies. For statistical analysis of assembly properties
473 we treated each assembly as a unit. For the area spanned by a given assembly, we first pro-
474 jected all assembly neurons on to the major axis of a fitted ellipse which occupied the NP of the
475 tectum. The normalised distance between the most anterior and posterior assembly members
476 was used to measure the span of the assembly. For assembly tuning, we calculated the mean
477 tuning properties of all neurons belonging to a given assembly.

478 *Decoding analysis:* To assess how well we could decode the stimulus angle from the re-
479 sponses, we used a Maximum Likelihood decoder (ML) as described in [77]. We assumed
480 that each neuron's response to a given stimulus s_j was independent, therefore, $P(R|s_j) =$
481 $\prod_{i=1}^N P(r_i|s_j)$. We then estimated the conditional probability that each cell i had the response
482 r_i to a given stimulus s_j as $P(r_i|s_j)$. $P(r_i|s_j)$ was estimated using the MATLAB *ksdensity* func-
483 tion. The decoded stimulus was the stimulus that gave the highest probability of evoking a
484 given population response, $S_{ML} = \operatorname{argmax}_j P(\vec{r}|s_j)$. A leave-one-out strategy was used for cross
485 validation: the probability distributions were estimated with all-but-one trials and we found the
486 stimulus that gives the highest probability to the response that was not included in the estima-
487 tion, and this process was repeated for each individual trial left out. The decoder performance
488 was calculated as the proportion of correctly identified stimuli out of the 9 stimuli presented.
489 For each stimulus we calculated mean performance, and for each fish we calculated mean
490 performance across all stimuli.

491 *Coactivity pattern*: To obtain significant coactivity levels we established a threshold using
492 the coactivity patterns during SA. We took the binarised activity pattern and randomly circularly
493 shifted the pattern 1000 times along the time axis, thus preserving the total activity level. The
494 threshold was chosen as the 95th percentile of the shuffled coactivity level. Frames of significant
495 coactivity were collected and divided into different response epochs for further analysis. We
496 applied PCA analysis on the coactivity patterns from different response epochs to quantify the
497 dimensionality of these responses epochs. The similarity between these coactivity pattern was
498 measured by cosine distance. Geometrical relations between EA and SA, SE patterns were
499 measured as the residuals of projections of SA, SE patterns onto the orthonormal basis of EA
500 patterns.

501 **Visual environment preference assay**

502 Fish embryos from the same clutch (either WT or *fmr1*^{-/-}) were split into two equally sized
503 groups and reared separately to control for inter-clutch variability across rearing conditions.
504 One group were reared in the naturalistic sensory environment (N) and the other in the reduced
505 sensory stimulation environment (R). Fish were reared until 8 or 9 dpf. Four fish from one of
506 the groups were then placed in a custom circular arena (see below). Free swimming behaviour
507 of the fish was recorded for 20 minutes continuously. Identical imaging was then performed for
508 the second group (*fmr1*^{-/-}: n=20, 20 fish; WT: n=16, 16 fish; for (N) and (R) rearing condition
509 respectively).

510 The arena was of the same dimensions as the petri dish in which the fish were reared
511 (diameter 85 mm and water depth 5 mm). The arena was made by filling a larger petri dish with
512 1.2% agrose (UltraPure, Invitrogen) and then cutting a well in the agarose using a 85mm petri
513 dish. A color photographic image of the gravel used for the naturalistic rearing environment,
514 scaled 1:1, was fixed to the underside of one half of the arena. For the other half of the arena we
515 fixed a flat color background which matched the mean hue and brightness of the gravel image
516 (Fig S3a). This image was constructed by randomly shuffling the coordinates of the pixels in the
517 gravel image then smoothing using a 2-dimensional Gaussian filter. The arena was placed onto
518 a custom-made imaging stage illuminated from the side using a stripe of white LED. Images

519 were recorded using a CMOS camera (GrasshopperGS3-U3-23S6M-C, Point Grey) with a 25
520 mm lens (C-Mount Lens FL-CC2514A-2M, Ricoh), at a rate of 100 fps.

521 Video data was compressed for convenience using an h264 codec with baseline en-
522 coding and quality parameter 17, resulting in visually lossless compression. The position of
523 each fish was tracked using custom software written in MATLAB. The background image was
524 first subtracted by adaptive per-pixel Gaussian modelling on a sliding window comprising every
525 400th frame spanning a total of 40000 frames (6 minutes and 40 seconds), with a foreground
526 threshold of 2 standard deviations above the mean pixel value. Additionally, a pixel was only
527 considered foreground if its value was above the threshold in at least two of three temporally
528 adjacent frames (the current frame and the two previous frames). Erroneous foreground objects
529 with total area less than 8 pixels were removed using a connected components filter. Remain-
530 ing foreground object masks were spatially smoothed using a 2-dimensional Gaussian filter and
531 filtered again by connected components to keep only the 4 largest objects which correspond to
532 the four fish. The detected centroids were linked between frames based on minimum Euclidean
533 distance to obtain the trajectory for each fish. We then calculated a gravel preference measure
534 for each fish, defined as the proportion of time that the fish spent on the half of the dish with the
535 gravel substrate.

536 **Social behaviour assay**

537 Custom U-shaped chambers were constructed using a 3D printer. Chambers consisted
538 of 3 compartments separated by 2 glass walls; 2 'cue' compartments each sized 20×18 mm
539 and a 'test' compartment of length 45 mm (Fig. 7a). Chambers were illuminated using a white
540 LED light strip. A test fish (either WT or *fmr1*^{-/-}) was placed into the test compartment for 5 min
541 to adjust. A WT cue fish was then placed into the left cue compartments. Behavior of both fish
542 was then imaged using a CMOS camera (GrasshopperGS3-U3-23S6M-C, Point Grey) with a
543 25 mm lens (C-Mount Lens FL-CC2514A-2M, Ricoh) at 100 or 175 fps for 30 mins. For practical
544 reasons (the large number of fish involved and the relatively long rearing time) these fish were
545 raised in featureless dishes.

The locations of the cue and test fish were tracked using custom MATLAB software. Re-

gions of interest (ROIs) were manually drawn for the cue and test chambers respectively to track each fish separately. To model the background a mean image was created using every 500th frame of the movie. To extract a binary image of the fish in each frame, the background was subtracted and pixels with resulting values greater than zero were considered foreground. The location of each fish was computed as the centre of mass of the largest connected component in its corresponding ROI. We calculated the social preference index (SPI) as:

$$\text{SPI} = \frac{\text{Number of social frames} - \text{Number of non-social frames}}{\text{Total frames}}$$

546 where social frames and non-social frames were defined as a frames for which the test fish was
547 located within the social zone or non-social zone respectively, as shown in Fig. 7a. To quantify
548 the dynamics of fish interaction during social frames we adapted the software written in Python
549 from [47].

550 For each fish, we calculated the instantaneous speed (mm/s). We considered the cue
551 fish as the reference fish, and identified bout times as the peaks in speed over the full duration
552 of the recording. Peaks were defined as local maxima that were at least two standard deviations
553 greater than the fish's mean speed. We computed the bout triggered average (BTA) speed of
554 the test fish as the mean over all bouts of the speed of the test fish for the period spanning
555 200 ms either side of each peak. We quantified the average lag of any movement induced in
556 the test fish by the cue fish as the mean of the delay between each reference peak and the
557 next subsequent peak for the test fish. This process was then repeated with the test fish as the
558 reference.

559 **Statistical analysis**

560 The Jarque Bera test was used to determine whether data was normally distributed. If
561 any group of data was not normally distributed the Wilcoxon rank sum test was used at each age
562 group to compare effects between genotype. If all groups were normally distributed, ANOVA
563 was used followed by post-hoc t-tests.

564 **Acknowledgements**

565 **Funding:** This work was supported by a grant from the Simons Foundation (SFARI 569051,
566 GJG). Imaging was performed at the Queensland Brain Institutes Advanced Microscopy Facility
567 using a Zeiss LSM 710 2-photon microscope, supported by the Australian Government through
568 the ARC LIEF grant LE130100078.

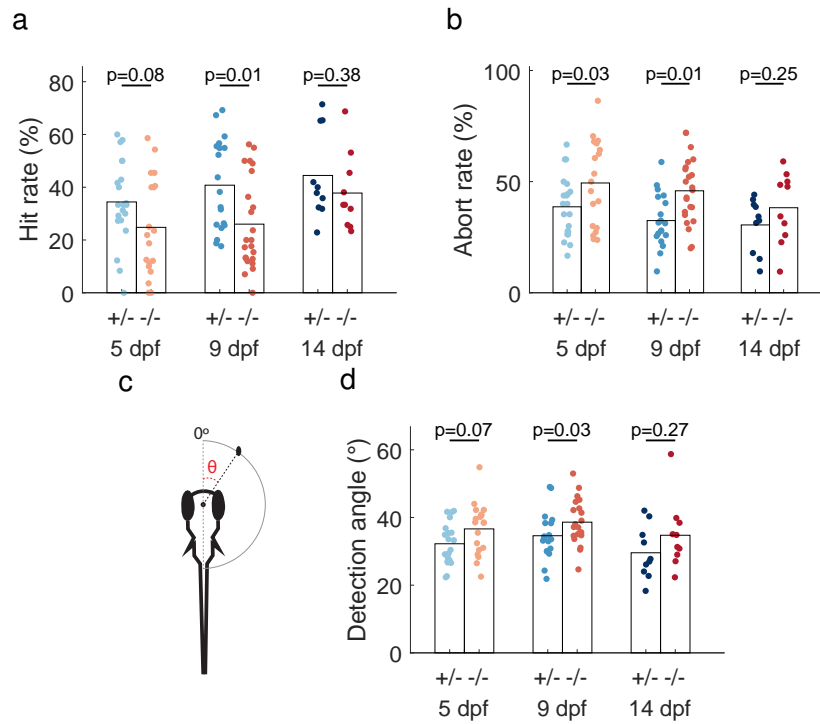


Figure 1: ***fmr1*^{-/-} fish show changes in hunting behavior.** **a.** At 9 dpf *fmr1*^{-/-} fish had a lower hit rate. **b.** At 5 and 9 dpf *fmr1*^{-/-} fish had a higher abort rate. **c.** Prey angle was defined as the angle between the midline of the fish and the location of the paramecium prior to eye convergence (for detection angle) or after the first bout (after-bout angle). **d.** 9 dpf *fmr1*^{-/-} fish responded to prey further towards the rear of the visual field.

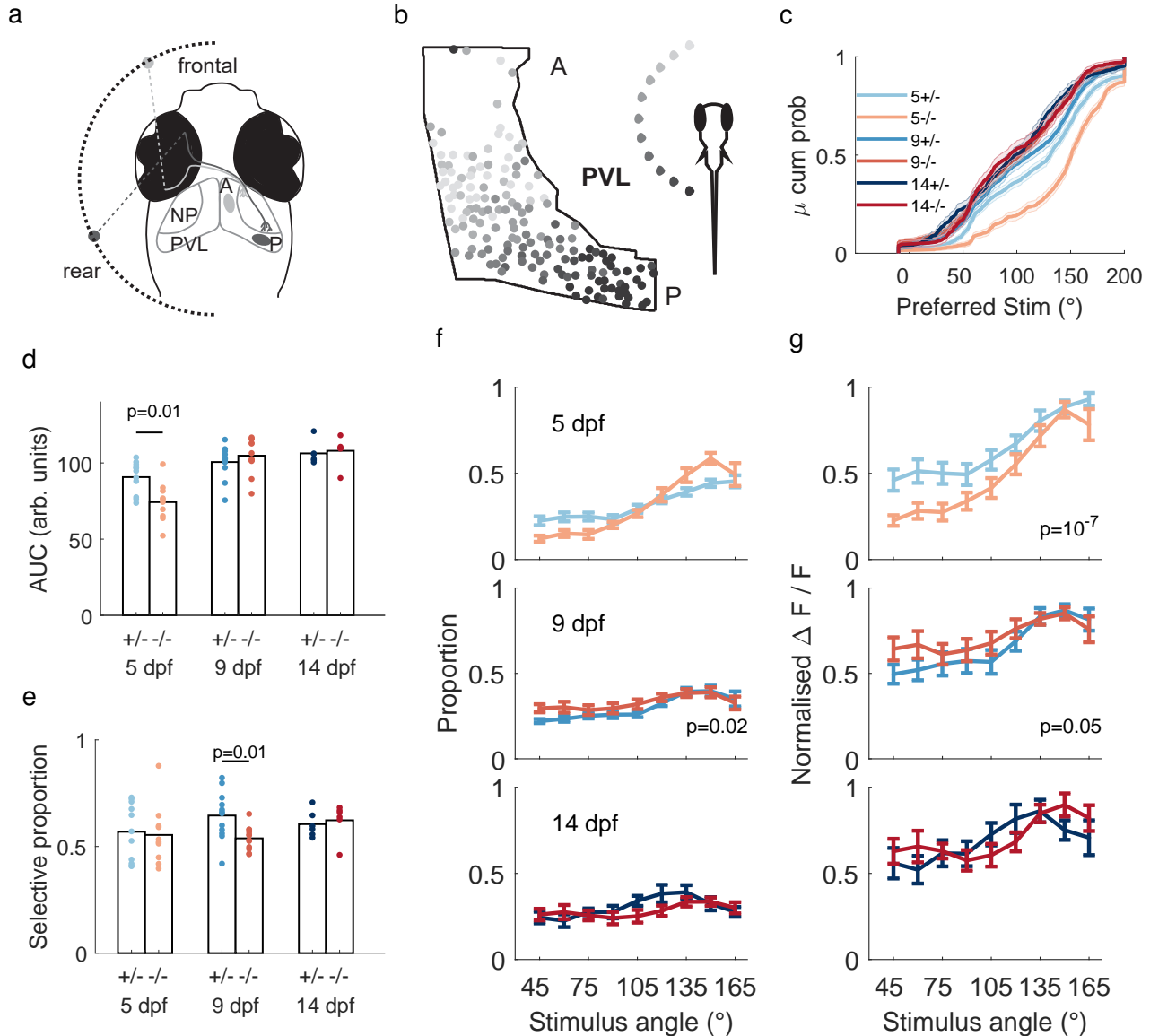


Figure 2: Tectal neurons in *fmr1*^{-/-} fish show altered activity statistics. **a.** Schematic of the retinotectal projection in zebrafish. Retinal ganglion cells in the nasal part of the retina, representing the rear visual field, project to the posterior part of the tectum (dark grey). Retinal ganglion cells in the temporal part of the retina, representing the frontal visual field, project to the anterior part of the tectum (light grey). NP: neuropil; PVL: periventricular layer; A: anterior; P: posterior. **b.** Retinotectal projections are organised topographically in *fmr1*^{-/-} fish (example 9-dpf fish). The stimulus position in the visual field to which each neuron in the PVL best responds is shown (see inset for grey-scale code). **c.** Cumulative distribution of preferred stimulus locations for both genotypes at 5, 9 and 14 dpf suggests a delay in 5-dpf *fmr1*^{-/-} fish. **d.** Area under the curves in **c** shows that 5 dpf *fmr1*^{-/-} fish had a less balanced representation of the visual field than 5-dpf *fmr1*^{+/-} fish. **e.** Proportion of stimulus-selective neurons was lower in *fmr1*^{-/-} fish at 9 dpf. **f.** Proportions of neurons responding to each stimulus angle were less balanced at 9 dpf for *fmr1*^{-/-} fish. **g.** Responses to anterior stimuli were weaker in 5 dpf *fmr1*^{-/-} fish. For **f,g** see panel c for color key. p-values indicate genotype effects using 2-way-ANOVA.

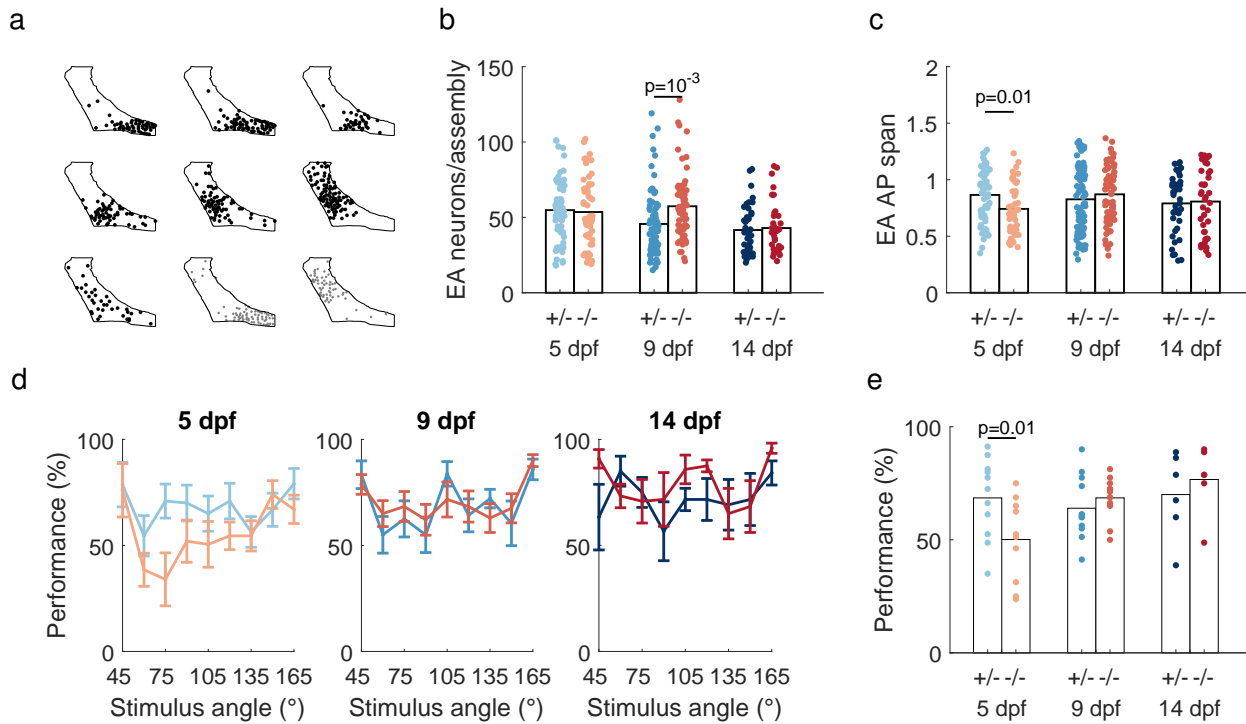


Figure 3: Neural assemblies and neural coding are altered in *fmr1*^{-/-} fish. **a.** The assemblies detected in an example 8 dpf *fmr1*^{-/-} fish drawn on the outline of the PVL. Black: EA assemblies. Gray: SA assemblies. **b.** At 9 dpf *fmr1*^{-/-} fish had more neurons per EA assembly than *fmr1*^{+/-} fish. **c.** At 5 dpf *fmr1*^{-/-} fish had more compact assemblies. **d.** Comparison of decoder performance as a function of visual field position between genotypes at 5, 9 and 14 dpf. Color code as in earlier panels. **e.** Decoder performance averaged over frontal spots (up to 90°) was lower in *fmr1*^{-/-} fish at 5 dpf.

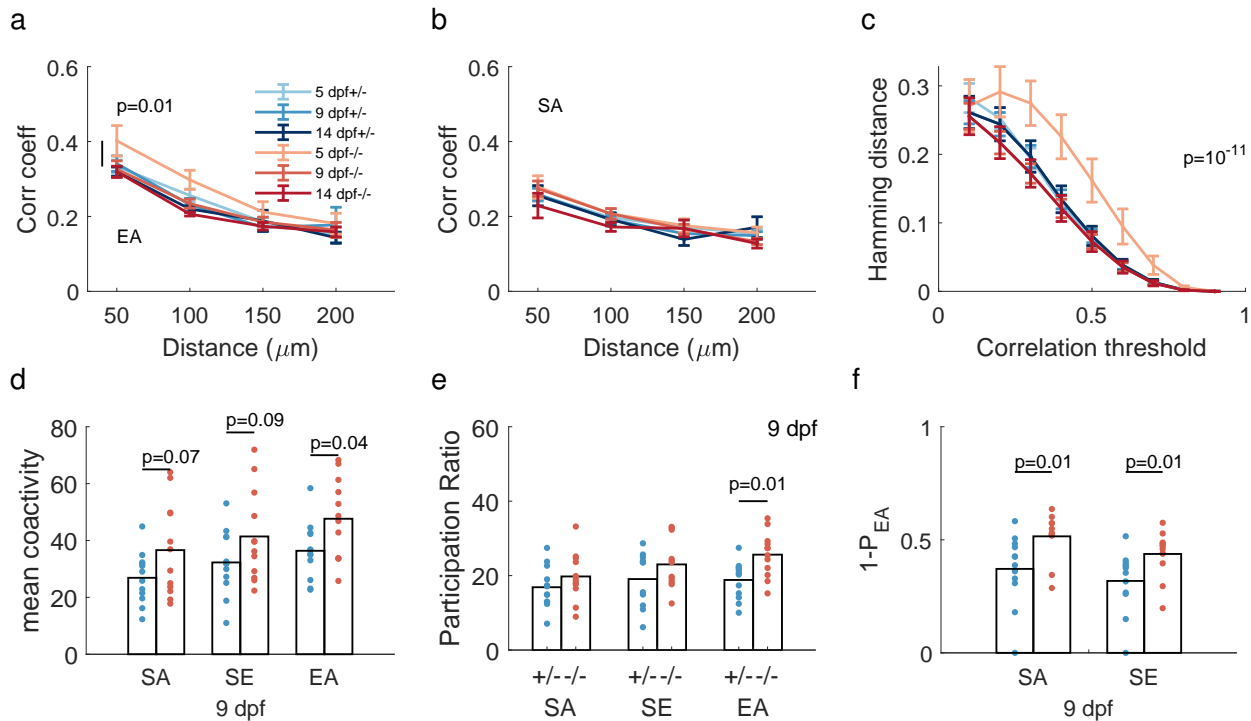


Figure 4: Network properties are altered in *fmr1*^{-/-} fish. **a.** At 5 dpf EA correlations were greater at short range ($<50 \mu\text{m}$) for *fmr1*^{-/-} fish. **b.** SA correlations were similar between genotypes. **c.** The similarity between EA and SA correlation structures was lower at 5 dpf for *fmr1*^{-/-} fish (color scheme as in a). **d.** The number of coactive neurons during EA at 9 dpf was higher for *fmr1*^{-/-} fish. **e.** The dimensionality of evoked activity at 9 dpf was higher for *fmr1*^{-/-} fish, as measured by the participation ratio. **f.** The residuals of the projections of SA and SE onto the EA space were larger in 9-dpf *fmr1*^{-/-} fish.

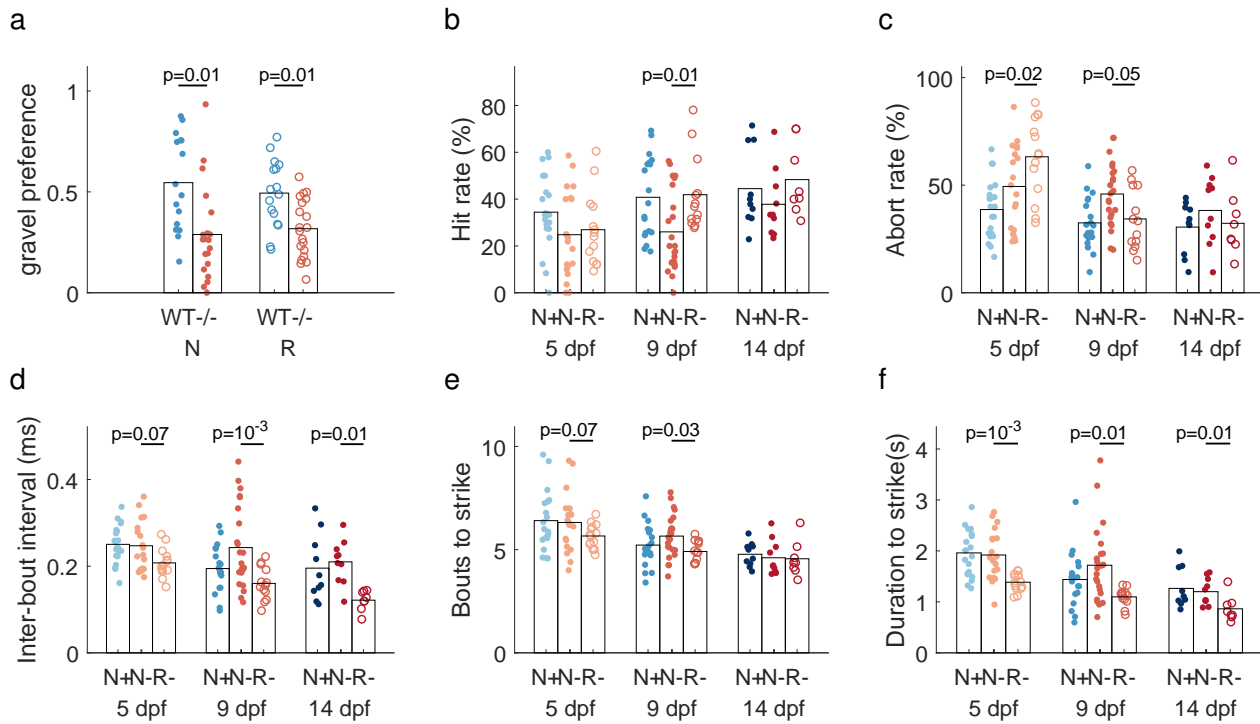


Figure 5: Reduced sensory stimulation improves hunting behaviours in *fmr1*^{-/-} fish. **a.** *fmr1*^{-/-} fish preferred a featureless to gravel environment, but *fmr1*^{+/-} fish had no preference. N: fish reared under naturalistic conditions; R: fish reared under reduced stimulation (featureless) conditions. p-values shown are 2-sample t-test. Results for 1-sample t-tests comparing each sample with 0.5 were 0.4 (N) and 0.9 (R) for WT, and 0.0007 (N) and 0.00002 (R) for *fmr1*^{-/-}. **b-f.** Terminology: R-, *fmr1*^{-/-} fish raised with reduced sensory stimulation; N-, *fmr1*^{-/-} fish raised under naturalistic conditions; N+, *fmr1*^{+/-} fish reared under naturalistic conditions (shown for comparison, same data as Figs 1-4). **b.** Hit ratio was higher for *fmr1*^{-/-}(R) than *fmr1*^{-/-}(N) fish at 9 dpf, towards the *fmr1*^{+/-}(N) case. **c.** Abort rate was greater for *fmr1*^{-/-}(R) than *fmr1*^{-/-}(N) fish at 5 dpf, but less at 9 dpf, towards the *fmr1*^{+/-}(N) case. **d-f.** *fmr1*^{-/-}(R) fish were more efficient in hunting than *fmr1*^{-/-}(N) fish with shorter inter-bout interval (9 and 14 dpf), less bouts to stike (9 dpf) and shorter duration to strike (all ages).

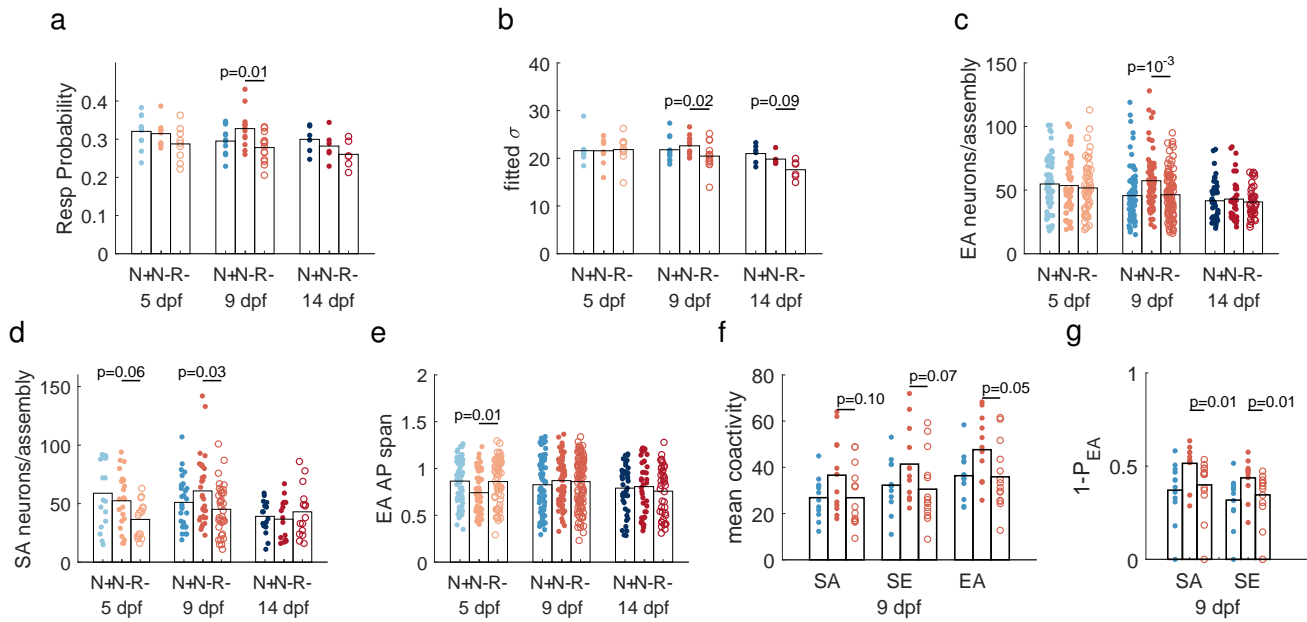


Figure 6: Reduced sensory stimulation in *fmr1*^{-/-} fish moves tectal activity closer to the *fmr1*^{+/-}(N) case. **a.** At 9 dpf neuron response probability was lower for *fmr1*^{-/-}(R) fish, towards the *fmr1*^{+/-}(N) case. **b.** At 9 dpf neurons in *fmr1*^{-/-}(R) fish had smaller tuning width compared to *fmr1*^{-/-}(N) fish, towards the *fmr1*^{+/-}(N) case. **c-d.** At 9 dpf *fmr1*^{-/-}(R) fish had less neurons per assembly for both EA (c) and SA (d) assemblies, towards the *fmr1*^{+/-}(N) case. **e.** EA assembly members spanned more of the AP axis in *fmr1*^{-/-}(R) fish at 5 dpf, towards the *fmr1*^{+/-}(N) case. **f.** 9 dpf *fmr1*^{-/-}(R) fish had lower coactivity levels than *fmr1*^{-/-}(N) fish for EA epochs, towards the *fmr1*^{+/-}(N) case. **g.** When projected onto the subspace of EA patterns, SA patterns of the 9 dpf *fmr1*^{-/-}(R) fish had smaller residuals, towards the *fmr1*^{+/-}(N) case.

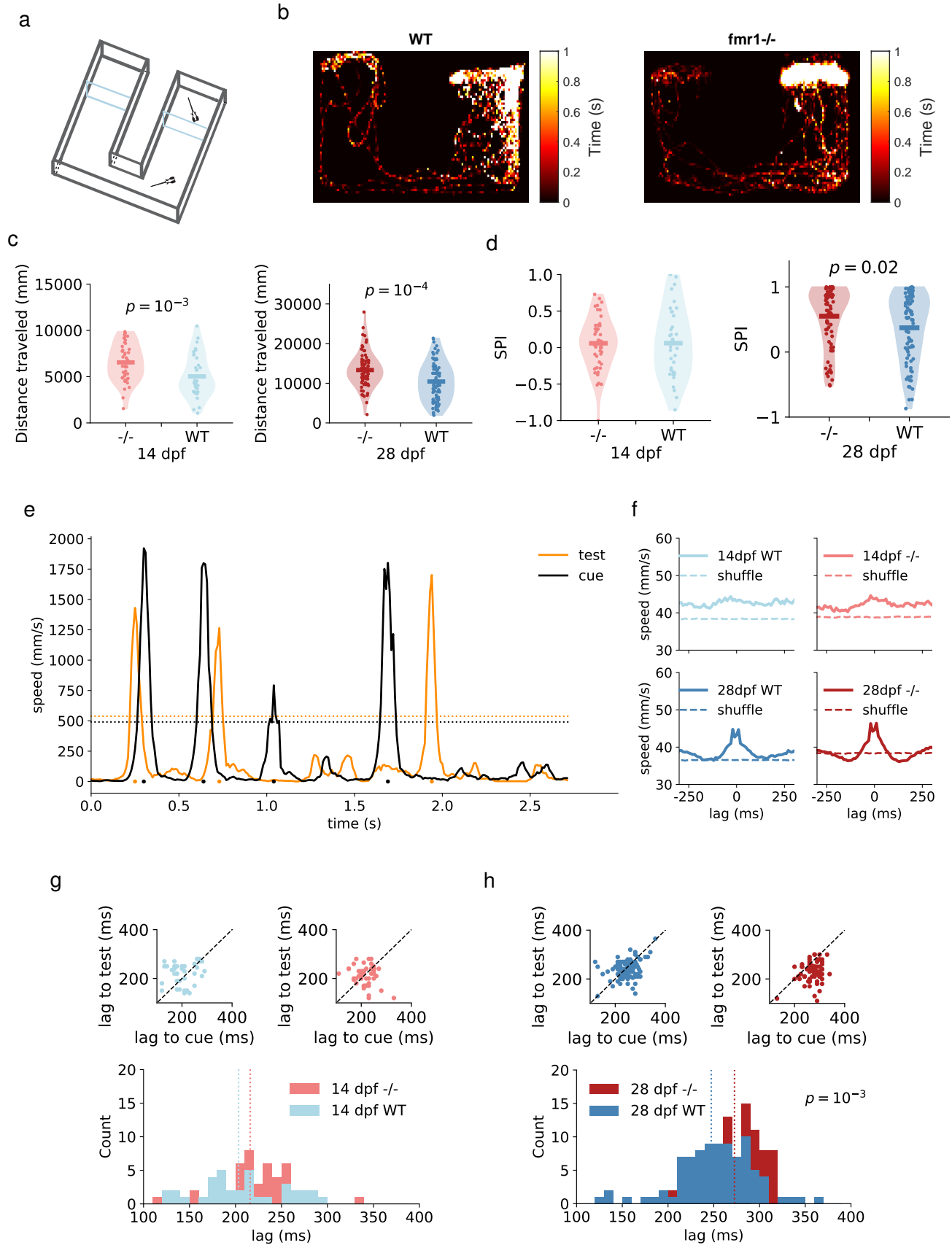
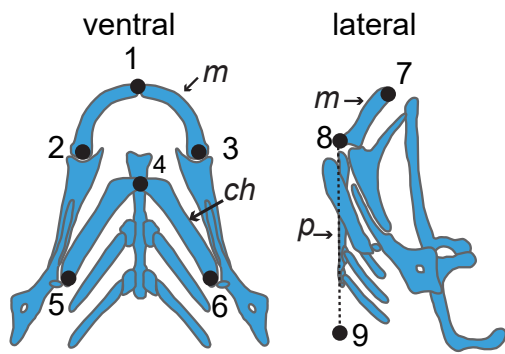


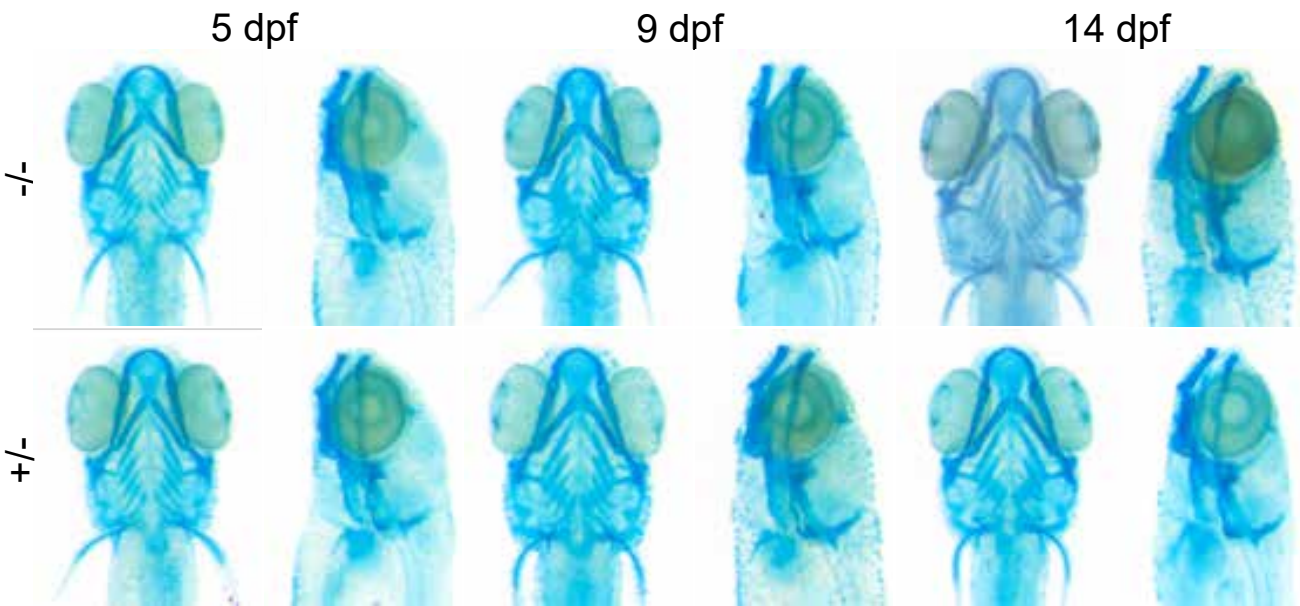
Figure 7: ***fmr1*^{-/-} fish display altered social behavior.** **a.** Illustration of the chamber used for the social assay. **b.** Example heat maps of the position of the test fish over 30 min (28 dpf, WT SPI: 0.75; *fmr1*^{-/-} SPI: 0.84). **c.** Total distance traveled was greater for *fmr1*^{-/-} than WT fish at both 14 and 28 dpf. **d.** At 28 dpf social preference index (SPI) was higher for *fmr1*^{-/-} fish. **e.** An example temporal segment of fish speed illustrating that the fish respond to each other's movements, and that either fish can lead. Dashed line represents significant motion threshold level. Each dot indicates a significant movement peak time. **f.** Averaged motion signal for 200 ms each side of movement peaks confirmed coordinated movements at 28 but not 14 dpf. **g - h.** Average movement lag was longer for *fmr1*^{-/-} fish at 28 dpf.

a

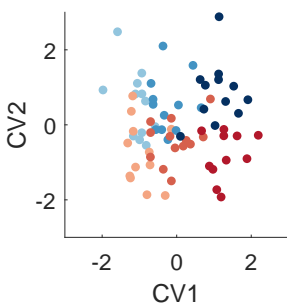


1. anterior point of Meckel's cartilage (ventral view)
 2. posterior end of the left Meckel's cartilage
 3. posterior end of the right Meckel's cartilage
 4. junction of the left and right ceratohyal cartilage
 5. posterior end the left ceratohyal cartilage
 6. posterior end the right ceratohyal cartilage
 7. anterior end of Meckel's cartilage (lateral view)
 8. junction of Meckel's cartilage and the palatoquadrate
 9. distal point along the lateral axis of the palatoquadrate
- m*: Meckel's cartilage; *ch*: ceratohyal cartilage; *p*: palatoquadrate.

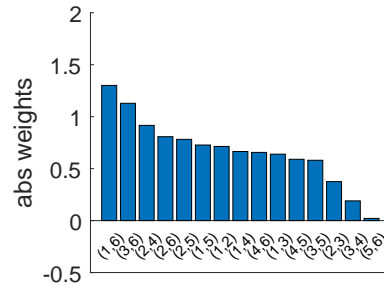
b



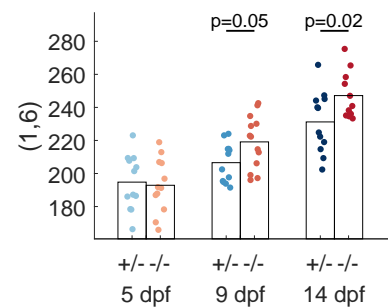
c



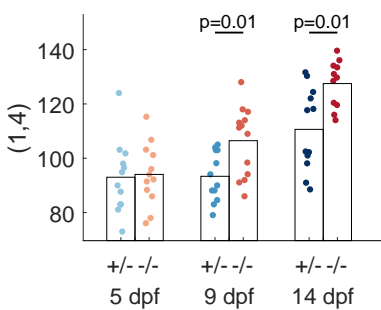
d



e



f



g

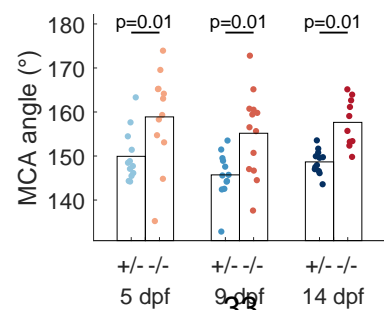


Figure S1. ***fmr1*^{-/-} fish show craniofacial abnormalities.** **a.** Schematic of the alcian blue-stained cartilages and the landmarks selected for analysis. **b.** Example image of Alcian blue staining of fish at 5, 9 and 14 dpf (*fmr1*^{-/-}: n = 12, 12, 12; *fmr1*^{+/-}: n = 12, 13, 10, for each age respectively). **c.** CVA analysis revealed significant association between morphological traits and the age and genotype of the fish. CV1 reflects correlation with age ($p = 10^{-15}$; magnitude of canonical coefficients $|b_{CV1,age}| = 2.45$ and $|b_{CV1,genotype}| = 0.20$; See Methods). CV2 reflects correlation with genotype ($p = 10^{-4}$; $|b_{CV2,age}| = 0.20$ and $|b_{CV2,genotype}| = 1.98$). **d.** The magnitude of the weights of CV2 for different distances between the landmarks on the ventral view. **e.** The distance with the highest weight, (1, 6), was larger in *fmr1*^{-/-} fish at 9 and 14 dpf. **f.** The distance (1, 4), equivalent to lower jaw length, was larger in *fmr1*^{-/-} fish at 9 and 14 dpf. **g.** The Meckel's cartilage angle (MCA, between points 7, 8, and 9) was less acute in *fmr1*^{-/-} fish.

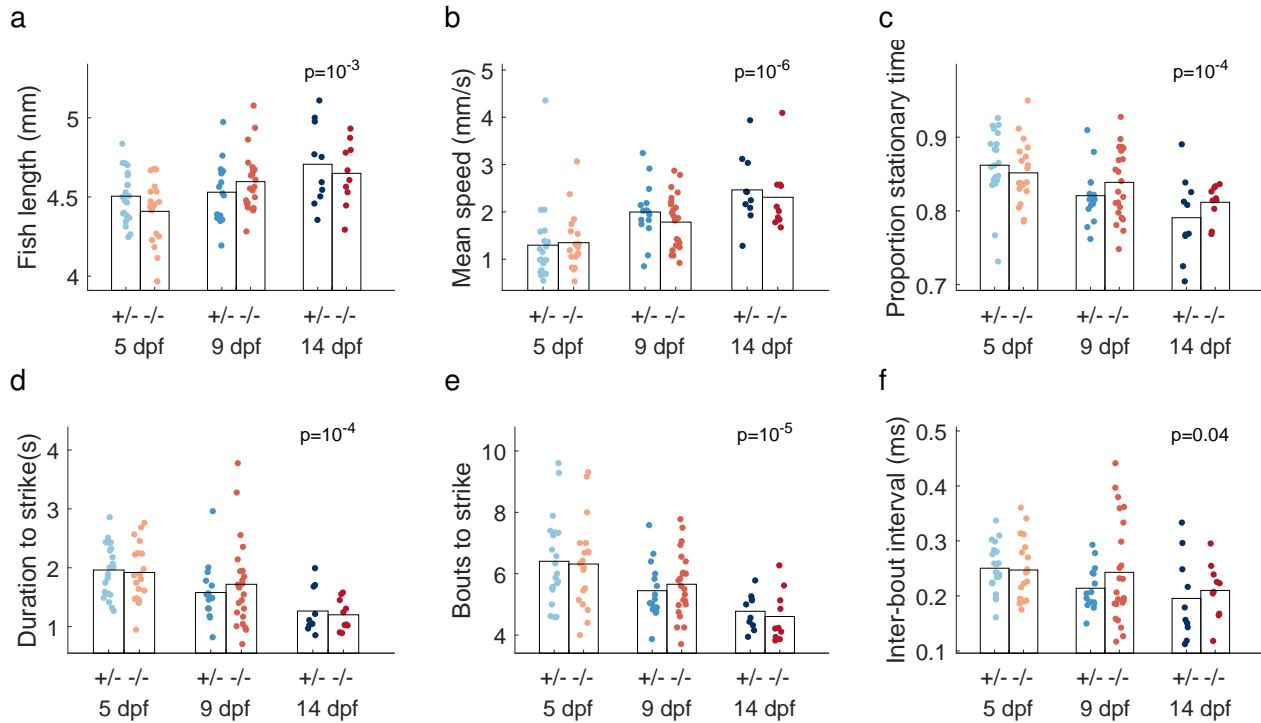


Figure S2. ***fmr1*^{-/-} fish did not show any motor deficits during hunting.** **a-c.** Fish length, mean swimming speed, and the proportion of stationary time during hunting was similar between genotypes. **d-f.** The duration to strike, the number of bouts made before a strike and the inter-bout interval during a hunting sequence were not different between genotypes. All measures showed significant differences with age (p values show age effect from one-way ANOVA), indicating a development trend of more efficient hunting over age.

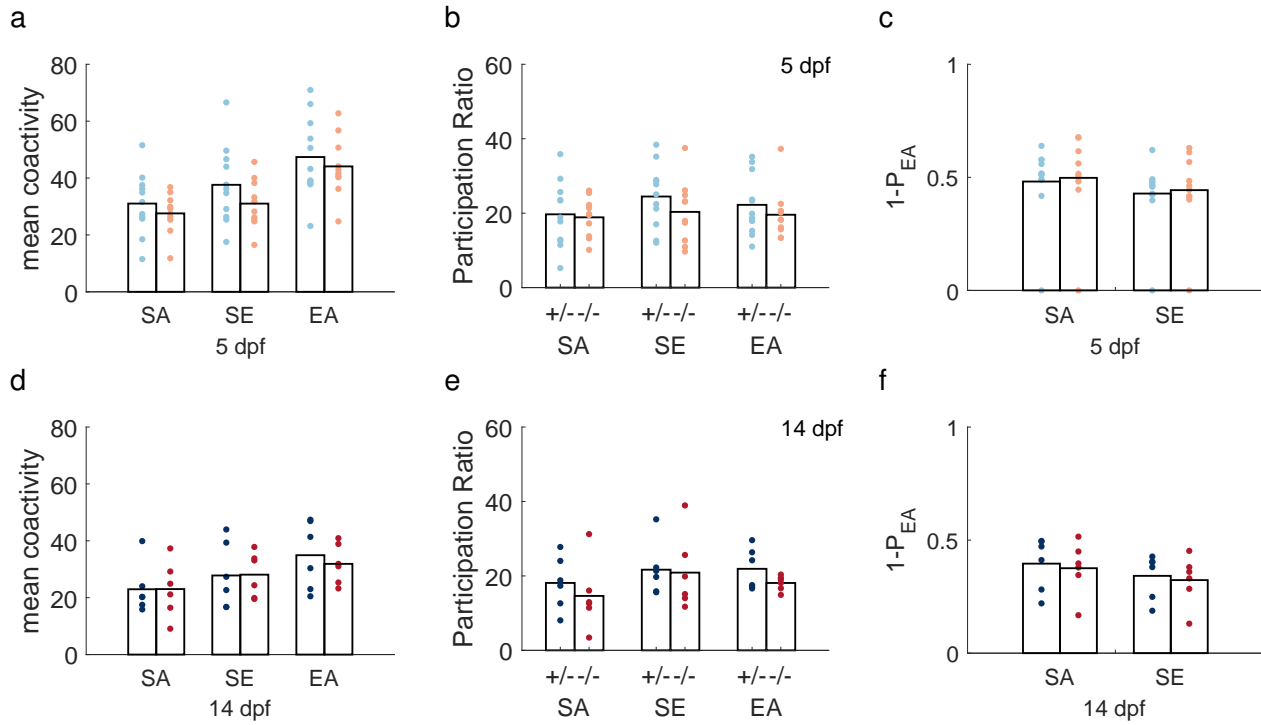


Figure S3. **Tectal coactivity patterns were not altered in *fmr1*^{-/-} fish at 5 and 14 dpf.** **a-c.** Mean coactivity level, participation ratio and residuals of SA and SE patterns on EA patterns at 5 dpf. **d-f.** Same measures at 14 dpf. There were no significant differences between genotypes.



Figure S4. **Gravel preference was independent of rearing condition.** **a.** The image placed underneath the dish in which the fish were swimming. The featureless side (left) of the image was produced by scrambling and smoothing the gravel image (right) to ensure average brightness and color are matched (see Methods). **b.** Rearing condition did not affect the gravel preference of either genotype.

References

- [1] Robertson CE, Baron-Cohen S (2017) Sensory perception in autism. *Nature Reviews Neuroscience* 18(11):671–684.
- [2] Estes A, et al. (2015) Behavioral, cognitive, and adaptive development in infants with autism spectrum disorder in the first 2 years of life. *Journal of Neurodevelopmental Disorders* 7(1):24.
- [3] O'Donnell WT, Warren ST (2002) A decade of molecular studies of Fragile X syndrome. *Annual Review of Neuroscience* 25(1):315–338.
- [4] Bassell GJ, Warren ST (2008) Fragile X syndrome: loss of local mrna regulation alters synaptic development and function. *Neuron* 60(2):201–214.
- [5] Contractor A, Klyachko VA, Portera-Cailliau C (2015) Altered neuronal and circuit excitability in Fragile X syndrome. *Neuron* 87(4):699 – 715.
- [6] Razak KA, Dominick KC, Erickson CA (2020) Developmental studies in Fragile X syndrome. *Journal of Neurodevelopmental Disorders* 12(1):13.
- [7] Hunter J, et al. (2014) Epidemiology of Fragile X syndrome: A systematic review and meta-analysis. *American Journal of Medical Genetics Part A* 164(7):1648–1658.
- [8] Hagerman RJ, et al. (2017) Fragile X syndrome. *Nature Reviews Disease Primers* 3(1):17065.
- [9] Kogan CS, et al. (2004) Integrative cortical dysfunction and pervasive motion perception deficit in Fragile X syndrome. *Neurology* 63(9):1634–1639.
- [10] Scerif G, Cornish K, Wilding J, Driver J, Karmiloff-Smith A (2004) Visual search in typically developing toddlers and toddlers with fragile X or Williams syndrome. *Developmental Science* 7(1):116–130.
- [11] Baranek GT, et al. ((2008) Developmental trajectories and correlates of sensory processing in young boys with Fragile X syndrome. *Physical & Occupational Therapy In Pediatrics* 28(1):79–98.

- [12] Farzin F, Whitney D, Hagerman R, Rivera S (2008) Contrast detection in infants with Fragile X syndrome. *Vision Research* 48(13):1471 – 1478.
- [13] Simmons DR, et al. (2009) Vision in autism spectrum disorders. *Vision Research* 49(22):2705 – 2739.
- [14] Farzin F, Rivera SM, Whitney D (2011) Resolution of spatial and temporal visual attention in infants with Fragile X syndrome. *Brain : A Journal of Neurology* 134(Pt 11):3355–3368.
- [15] Marco EJ, Hinkley LBN, Hill SS, Nagarajan SS (2011) Sensory processing in autism: a review of neurophysiologic findings. *Pediatric Research* 69(5 Pt 2):48–54.
- [16] Orefice LL, et al. (2016) Peripheral mechanosensory neuron dysfunction underlies tactile and behavioral deficits in mouse models of ASDs. *Cell* 166(2):299 – 313.
- [17] Kleinhans NM, et al. (2009) Reduced neural habituation in the amygdala and social impairments in autism spectrum disorders. *American Journal of Psychiatry* 166(4):467–475.
- [18] Puts NAJ, Wodka EL, Tommerdahl M, Mostofsky SH, Edden RAE (2014) Impaired tactile processing in children with autism spectrum disorder. *Journal of Neurophysiology* 111(9):1803–1811.
- [19] Ethridge LE, et al. (2016) Reduced habituation of auditory evoked potentials indicate cortical hyper-excitability in Fragile X syndrome. *Translational Psychiatry* 6(4):e787–e787.
- [20] Gonçalves JT, Anstey JE, Golshani P, Portera-Cailliau C (2013) Circuit level defects in the developing neocortex of fragile X mice. *Nature Neuroscience* 16(7):903–909.
- [21] Zhang Y, et al. (2014) Dendritic channelopathies contribute to neocortical and sensory hyperexcitability in *Fmr1^{ly}* mice. *Nature Neuroscience* 17(12):1701–1709.
- [22] Arnett MT, Herman DH, McGee AW (2014) Deficits in tactile learning in a mouse model of Fragile X syndrome. *PLOS ONE* 9(10):1–7.
- [23] He CX, et al. (2017) Tactile defensiveness and impaired adaptation of neuronal activity in the *fmr1* knock-out mouse model of autism. *Journal of Neuroscience* 37(27):6475–6487.

- [24] Bianco I, Kampff A, Engert F (2011) Prey capture behavior evoked by simple visual stimuli in larval zebrafish. *Frontiers in Systems Neuroscience* 5:101.
- [25] Muto A, Kawakami K (2013) Prey capture in zebrafish larvae serves as a model to study cognitive functions. *Frontiers in Neural Circuits* 7:110.
- [26] Bianco IH, Engert F (2015) Visuomotor transformations underlying hunting behavior in zebrafish. *Current biology* 25(7):831–846.
- [27] Avitan L, et al. (2020) Behavioral signatures of a developing neural code. *Current Biology* 30(17):3352 – 3363.
- [28] Bolton AD, et al. (2019) Elements of a stochastic 3d prediction engine in larval zebrafish prey capture. *eLife* 8:e51975.
- [29] Larsch J, Baier H (2018) Biological motion as an innate perceptual mechanism driving social affiliation. *Current Biology* 28(22):3523 – 3532.
- [30] Ahrens MB, et al. (2012) Brain-wide neuronal dynamics during motor adaptation in zebrafish. *Nature* 485(7399):471–477.
- [31] Ahrens MB, Orger MB, Robson DN, Li JM, Keller PJ (2013) Whole-brain functional imaging at cellular resolution using light-sheet microscopy. *Nature Methods* 10(5):413–420.
- [32] Stewart AM, Nguyen M, Wong K, Poudel MK, Kalueff AV (2014) Developing zebrafish models of autism spectrum disorder (ASD). *Progress in Neuro-Psychopharmacology and Biological Psychiatry* 50:27 – 36.
- [33] Restivo L, et al. (2005) Enriched environment promotes behavioral and morphological recovery in a mouse model for the Fragile X syndrome. *Proceedings of the National Academy of Sciences* 102(32):11557–11562.
- [34] Lauterborn JC, Jafari M, Babayan AH, Gall CM (2013) Environmental enrichment reveals effects of genotype on hippocampal spine morphologies in the mouse model of Fragile X syndrome. *Cerebral Cortex* 25(2):516–527.

- [35] den Broeder MJ, et al. (2009) Generation and characterization of *fmr1* knockout zebrafish (*fmr1* mutant zebrafish. *PLoS ONE* 4(11):e7910.
- [36] Heulens I, et al. (2013) Craniofacial characteristics of Fragile X syndrome in mouse and man. *European Journal of Human Genetics* 21(8):816–823.
- [37] Tucker B, Richards RI, Lardelli M (2006) Contribution of mGluR and *Fmr1* functional pathways to neurite morphogenesis, craniofacial development and Fragile X syndrome. *Human Molecular Genetics* 15(23):3446–3458.
- [38] Hu J, et al. (2020) Hyperactivity, memory defects, and craniofacial abnormalities in zebrafish *fmr1* mutant larvae. *Behavior Genetics* 50(3):152–160.
- [39] Zelditch ML, Swiderski DL, Sheets HD, Fink WL (2004) *Geometric Morphometrics for Biologists* eds. Zelditch ML, Swiderski DL, Sheets HD, Fink WL. (Academic Press, San Diego).
- [40] Gahtan E, Tanger P, Baier H (2005) Visual prey capture in larval zebrafish is controlled by identified reticulospinal neurons downstream of the tectum. *Journal of Neuroscience* 25(40):9294–9303.
- [41] Buzsáki G (2010) Neural syntax: Cell assemblies, synapse ensembles, and readers. *Neuron* 68(3):362 – 385.
- [42] Avitan L, et al. (2017) Spontaneous Activity in the Zebrafish Tectum Reorganizes over Development and Is Influenced by Visual Experience. *Current Biology* 27(16):2407 – 2419.
- [43] Gao P, et al. (2017) A theory of multineuronal dimensionality, dynamics and measurement. *bioRxiv* <https://doi.org/10.1101/214262>.
- [44] Sainsbury T, Diana G, Meyer M (2018) The organisation, dynamics and development of neural assemblies in the tectum. Program No. 553.04. 2018 Neuroscience Meeting Planner. San Diego, CA: Society for Neuroscience, 2018. Online.

- [45] Schroeder P, Jones S, Young IS, Sneddon LU (2014) What do zebrafish want? Impact of social grouping, dominance and gender on preference for enrichment. *Laboratory Animals* 48(4):328–337.
- [46] Tavassoli T, Miller LJ, Schoen SA, Nielsen DM, Baron-Cohen S (2014) Sensory over-responsivity in adults with autism spectrum conditions. *Autism* 18(4):428–432.
- [47] Dreosti E, Lopes G, Kampff A, Wilson S (2015) Development of social behavior in young zebrafish. *Frontiers in Neural Circuits* 9:39.
- [48] Ng MC, Yang YL, Lu KT (2013) Behavioral and synaptic circuit features in a zebrafish model of Fragile X syndrome. *PLOS ONE* 8(3):1–8.
- [49] Wu YJ, et al. (2017) Fragile X mental retardation-1 knockout zebrafish shows precocious development in social behavior. *Zebrafish* 14(5):438–443.
- [50] Kim L, et al. (2014) Anxiety, hyperactivity and stereotypy in a zebrafish model of Fragile X Syndrome and autism spectrum disorder. *Progress in Neuro-Psychopharmacology and Biological Psychiatry* 55:40 – 49.
- [51] Shamay-Ramot A, et al. (2015) Fmrp interacts with adar and regulates RNA editing, synaptic density and locomotor activity in zebrafish. *PLOS Genetics* 11(12):1–28.
- [52] Constantin L, et al. (2020) Altered brain-wide auditory networks in a zebrafish model of Fragile X syndrome. *BMC Biology* 18(1):125.
- [53] Cheyne JE, Zabouri N, Baddeley D, Lohmann C (2019) Spontaneous activity patterns are altered in the developing visual cortex of the fmr1 knockout mouse. *Frontiers in Neural Circuits* 13:57.
- [54] Lee E, Lee J, Kim E (2017) Excitation/inhibition imbalance in animal models of autism spectrum disorders. *Biological Psychiatry* 81(10):838 – 847.
- [55] Cea-Del Rio CA, Huntsman MM (2014) The contribution of inhibitory interneurons to circuit dysfunction in Fragile X syndrome. *Frontiers in Cellular Neuroscience* 8:245.

- [56] Braat S, Kooy RF (2015) The GABA_A receptor as a therapeutic target for neurodevelopmental disorders. *Neuron* 86(5):1119 – 1130.
- [57] Berzhanskaya J, et al. (2016) Disrupted cortical state regulation in a rat model of Fragile X syndrome. *Cerebral Cortex* 27(2):1386–1400.
- [58] Goel A, et al. (2018) Impaired perceptual learning in a mouse model of Fragile X syndrome is mediated by parvalbumin neuron dysfunction and is reversible. *Nature Neuroscience* 21(10):1404–1411.
- [59] Antoine MW, Langberg T, Schnepel P, Feldman DE (2019) Increased excitation-inhibition ratio stabilizes synapse and circuit excitability in four autism mouse models. *Neuron* 101(4):648 – 661.
- [60] Robles E, Smith S, Baier H (2011) Characterization of genetically targeted neuron types in the zebrafish optic tectum. *Frontiers in Neural Circuits* 5:1.
- [61] Perche O, et al. (2018) Early retinal defects in *fmr1/y* mice: Toward a critical role of visual dys-sensitivity in the fragile x syndrome phenotype? *Frontiers in Cellular Neuroscience* 12:96.
- [62] Felgerolle C, et al. (2019) Visual behavior impairments as an aberrant sensory processing in the mouse model of fragile x syndrome. *Frontiers in Behavioral Neuroscience* 13:228.
- [63] Kogan CS, et al. (2004) Differential impact of the FMR1 gene on visual processing in fragile X syndrome. *Brain* 127(3):591–601.
- [64] Lagogiannis K, Diana G, Meyer MP (2020) Learning steers the ontogeny of an efficient hunting sequence in zebrafish larvae. *eLife* 9:e55119.
- [65] Oldfield CS, et al. (2020) Experience, circuit dynamics, and forebrain recruitment in larval zebrafish prey capture. *eLife* 9:e56619.
- [66] Rais M, Binder DK, Razak KA, Ethell IM (2018) Sensory processing phenotypes in Fragile X syndrome. *ASN Neuro* 10:1759091418801092.

- [67] Meredith RM, Holmgren CD, Weidum M, Burnashev N, Mansvelder HD (2007) Increased threshold for spike-timing-dependent plasticity is caused by unreliable calcium signaling in mice lacking fragile X gene *fmr1*. *Neuron* 54(4):627 – 638.
- [68] Meredith R (2015) Sensitive and critical periods during neurotypical and aberrant neurodevelopment: A framework for neurodevelopmental disorders. *Neuroscience & Biobehavioral Reviews* 50:180 – 188.
- [69] McConnell SR (2002) Interventions to facilitate social interaction for young children with autism: Review of available research and recommendations for educational intervention and future research. *Journal of Autism and Developmental Disorders* 32(5):351–372.
- [70] Hong MP, et al. (2019) Differentiating social preference and social anxiety phenotypes in Fragile X syndrome using an eye gaze analysis: a pilot study. *Journal of Neurodevelopmental Disorders* 11(1):1.
- [71] Gonzales-Rojas R, et al. (2020) The mouse model of fragile x syndrome exhibits deficits in contagious itch behavior. *Scientific Reports* 10(1):17679.
- [72] Rudie JD, et al. (2011) Reduced functional integration and segregation of distributed neural systems underlying social and emotional information processing in autism spectrum disorders. *Cerebral Cortex* 22(5):1025–1037.
- [73] Kappel J, Larsch J, Donovan J, Baier H (2019) A neural circuit for processing social motion cues in the juvenile zebrafish brain. *Cosyne Abstracts 2019*. Lisbon, Portugal.
- [74] Bolme DS, Beveridge JR, Draper BA, Lui YM (2010) Visual object tracking using adaptive correlation filters in *2010 IEEE Computer Society Conference on Computer Vision and Pattern Recognition*. pp. 2544–2550.
- [75] Felzenszwalb PF, Girshick RB, McAllester D, Ramanan D (2009) Object detection with discriminatively trained part-based models. *IEEE transactions on pattern analysis and machine intelligence* 32(9):1627–1645.
- [76] Mölter J, Avitan L, Goodhill GJ (2018) Detecting neural assemblies in calcium imaging data. *BMC Biology* 16(1):143.

[77] Avitan L, Pujic Z, Hughes NJ, Scott EK, Goodhill GJ (2016) Limitations of neural map topography for decoding spatial information. *Journal of Neuroscience* 36(19):5385–5396.